Constraining uncertainty in aerosol direct forcing

D. Watson-Parris[1], N Bellouin[2], L. Deaconu[1], N. Schutgens[3], M. Yoshioka[4], L. A. Regayre[4], K. J. Pringle[4], J. S. Johnson[4], K. S. Carslaw[4] and P. Stier[1]

[1]Atmospheric, Oceanic and Planetary Physics, Department of Physics, University of Oxford, Oxford, UK.

[2]Department of Meteorology, University of Reading, Reading, UK

[3]Earth Sciences, Faculty of Science, Vrije Universiteit Amsterdam

[4]School of Earth and Environment, University of Leeds, Leeds, UK.

Corresponding author: Duncan Watson-Parris (duncan.watson-parris@physics.ox.ac.uk)

Key Points:

- A strong relationship is demonstrated between total present-day aerosol loading and the anthropogenic contribution, across a variety of models.
- Observations of the total present-day aerosol loading are thus used to constrain uncertainty in anthropogenic aerosol and aerosol direct forcing
- Applying these constraints to one million samples of a 26-parameter perturbed parameter ensemble leads to a clear-sky RF_{ari} estimate of -0.67 ± 0.13 Wm^{-2}.

Abstract

The uncertainty in present-day anthropogenic forcing is dominated by uncertainty in the strength of the contribution from aerosol. Much of the uncertainty in the direct aerosol forcing can be attributed to uncertainty in the anthropogenic fraction of aerosol in the present-day atmosphere, due to a lack of historical observations. Here we present a robust relationship between total present-day aerosol optical depth and the anthropogenic contribution across two multi-model ensembles and a large single-model perturbed parameter ensemble. Using observations of aerosol optical depth, we determine a reduced likely range of the anthropogenic component and hence a reduced uncertainty in the direct forcing of aerosol.

Plain Language Summary

Despite the impacts of global warming already being felt around the world it is still unclear how much of the effect of greenhouse gasses is being offset by the cooling effect of atmospheric aerosol through the scattering of incoming sunlight and the modification of clouds. A large part of the difficulty in determining the effect of aerosol is in understanding the proportion of present-day aerosol that is due to human activity. In this work we demonstrate a strong relationship between the total amount of aerosol in the present-day atmosphere (something we can measure) and the amount due to human activity (something we cannot). We further show that this allows us to reduce the uncertainty in the cooling effect of aerosols.

1 Introduction

Aerosols affect the climate both directly by scattering and absorbing incoming solar radiation, and indirectly by providing the nuclei on which cloud droplets form. Anthropogenic perturbations to the natural background aerosol population can therefore change the balance in radiation at the top of the atmosphere and hence provide a forcing, which offsets some of the forcing due to anthropogenic greenhouse gasses. Despite a concerted effort since the last IPCC assessment (Myhre et al., 2013) the magnitude of anthropogenic aerosol forcing remains highly uncertain.

One of the main sources of uncertainty in aerosol forcing is the lack of reliable observational estimates of the amount of natural, or pre-industrial aerosol (Charlson et al., 1992; Carslaw et al., 2013; Carslaw et al., 2017). Discerning the anthropogenic contribution to present-day aerosol from present-day observations directly is challenging though. While some aerosol species, such as sea-salt, are easy to attribute to natural processes, others, such as sulfate and organic carbon, can have a variety of natural and anthropogenic sources. Further, non-linearities in some aerosol processes mean that anthropogenic perturbations can affect the production and removal of natural aerosol (Stier et al., 2006).

Aerosol optical depth ($\boldsymbol{\tau}$) is a measure of the extinction of solar radiation by aerosol and is directly related to the direct aerosol effect. Satellite remote sensing retrievals of $\boldsymbol{\tau}$ in the present day ($\boldsymbol{\tau_{PD}}$) are available from a wide range of sensors, on different platforms and using different retrieval algorithms. While satellite-based retrievals of $\boldsymbol{\tau}$ require accurate models of surface albedo and can suffer from biases due to the need to accurately screen for clouds, they are the only aerosol datasets available which provide near-global coverage over land and ocean. $\boldsymbol{\tau}$ is also a common GCM diagnostic, and a large ensemble of model values are available from the AeroCom modelling community (Myhre et al., 2013), as well as some contributions to the CMIP5 ensemble, making it an ideal observational constraint.

A number of cases have been found recently where relatively simple relationships between observable and unobservable quantities can be discerned, belying the apparent complexity of the underlying system (Allen & Ingram, 2002; Hall & Qu, 2006). These relationships can be exploited using observations to constrain model ensemble values of the unobservable quantity. Correlation does not imply causation, however, and so these 'emergent constraints' must be treated with care to ensure that the relationship is physically based and observationally robust. Further care should be taken that the ensemble of models used to sample the uncertainty adequately reflects the uncertainty in the properties in question. Similarly, perturbed parameter ensembles (PPEs) enable exploration of the parametric uncertainty, and with sufficient observations, a constrained estimate of a quantity from a given model. This method however can say little of the structural deficiencies of a model and large inter-model differences may be un-accounted for. Here we look to combine the strengths of each of these approaches in a complimentary way. An emergent constraint from a large multi-model ensemble is demonstrated, but not relied on. Instead a PPE is used to explore, and constrain, the parametric uncertainty quantitively in one model, in the context of the larger multi-model ensemble.

In this work we demonstrate, and explain, a robust relationship between $\boldsymbol{\tau_{PD}}$ and the anthropogenic aerosol optical depth, $\boldsymbol{\tau_{ant}}$ (defined as the difference between present-day and pre-industrial aerosol optical depth, denoted $\boldsymbol{\tau_{PD}}$ and $\boldsymbol{\tau_{PI}}$ respectively) across three different model ensembles. We use satellite-based observations of $\boldsymbol{\tau_{PD}}$ to constrain the uncertainty in $\boldsymbol{\tau_{ant}}$ in a large PPE, and in turn the clear-sky aerosol forcing (RF_{ari}).

2 A constraint emerges

As common GCM diagnostics, both $\boldsymbol{\tau_{PI}}$ and $\boldsymbol{\tau_{PD}}$ are available from a wide range of models. Here we consider the CMIP5 (Taylor et al., 2012) models which participated in the fixed sea surface temperature aerosol experiments (Zelinka et al., 2014) and the AeroCom Phase II models (Myhre et al., 2013). One drawback in using these ensembles to represent uncertainty in aerosol forcing however is that many of these simulations share anthropogenic emissions inventories and use the same or similar parameterizations for natural aerosol emissions, potentially leading to a lack of representativity within and across these ensembles. To sample these uncertainties, we use Gaussian Process (GP) emulators[1] (O'Hagan, 2006) trained on a perturbed parameter ensemble (PPE) of 183 simulations of HadGEM3-UKCA corresponding to distinct combinations of 26 physical parameters relating to aerosol processes and emissions, for both present-day (2008) and preindustrial (1850) emissions (Yoshioka et al., 2019; Carslaw et al., 2017). We are then able to explore the full parametric uncertainty attributable to the chosen parameter perturbations in global mean $\boldsymbol{\tau_{PI}}$ and $\boldsymbol{\tau_{PD}}$ by sampling the emulators at 1,000,000 parameter combinations from across the 26-dimensional parameter space of the PPE, drawn using a set of expert-elicited marginal distributions on the parameters (Yoshioka et al., 2019). Note that the three parameters relating to carbonaceous emissions were left unperturbed in this experiment as $\boldsymbol{\tau_{PD}}$ provides little constraint on these and they are only of secondary importance for RF_{ari}.

In order to account for the uncertainty in satellite observations of $\boldsymbol{\tau_{PD}}$ we use the standard deviation in the global mean value obtained from 7 distinct datasets covering 5 platforms, 3 sensors and 5 retrieval algorithms, as listed in Table 1. These observational datasets then provide well characterized global estimates of $\boldsymbol{\tau}$, although the possibility of remaining systematic biases cannot be entirely discounted. Due to the orbits of the platforms and the difficulty in retrieving $\boldsymbol{\tau}$ over snow and ice these values represent averages only between 60S and 60N.... For the PPE values reported here we consider the same latitudinal range. While using only the global yearly average of $\boldsymbol{\tau_{PD}}$ as a constraint allows considerable freedom in the spatial and temporal distribution in the model, we find it still provides a robust constraint, and minimizes observation and sampling uncertainties.

[1] The emulators are created using GPflow (Matthews et al. 2017) using a Gausian Process Regression model with a Radial Basis Function kernel and hyper-parameters optimized using the Broyden, Fletcher, Goldfarb, and Shanno (BFGS) algorithm (Nocedal and Wright 2006).

We consider all the sampled emulator variants whose $\boldsymbol{\tau_{PD}}$ is outside one standard deviation of the mean in the observed values implausible, and hence reject that parameter combination. The observed values are not normally distributed (since they are not truly independent, sharing instruments and retrieval algorithms) and this uncertainty range almost spans the entire observed values. In effect we are using a wide top-hat (or box-car) distribution for the observed $\boldsymbol{\tau_{PD}}$ (see Figure S1) and explore the sensitivity of our results to the width of this distribution below. This 'history matching' approach produces a 'constrained' set of model variants which is now compatible with the observations (see e.g. Lee et al. 2016). The parameter combinations corresponding to these plausible simulations are then used to predict unobservable quantities such as $\boldsymbol{\tau_{ant}}$ and RF_{ari}, providing the new, observationally constrained distributions.

Table 1: The satellite products and global mean values used to estimate the observational uncertainty in τ_{PD}

Platform	Sensor	Retrieval	AOD	Reference
Aqua	MODIS	DarkTarget	0.159	Levy et al. 2013
Terra	MODIS	DarkTarget	0.175	Ibid.
ENVISAT	AATSR	ADV	0.168	Kolmonen et al. 2016
ENVISAT	AATSR	ORAC	0.174	Thomas et al. 2009
ENVISAT	AATSR	SU	0.136	North et al. 2002
Noaa18	AVHRR	DeepBlue & SOAR	0.146	Hsu et al. 2013
Seastar	SeaWiFS	DeepBlue & SOAR	0.130	Ibid.
Mean			0.155	
Standard deviation			0.018	

Figure 1 shows the relationship between $\boldsymbol{\tau_{ant}}$ and $\boldsymbol{\tau_{PD}}$ in the CMIP5 and Aerocom multi-model ensembles, as well as the joint probability distribution for both the unconstrained HadGEM-UKCA PPE (contour lines) and the PPE constrained by the observations (as a hex-density plot[2]). The marginal distributions of $\boldsymbol{\tau_{ant}}$ and $\boldsymbol{\tau_{PD}}$ for each of the ensembles are shown along the top and right-hand-side. The distribution of $\boldsymbol{\tau_{PD}}$ in both the CMIP5 and AeroCom ensembles peaks just below the lower observational bounds, while the unconstrained PPE shows a larger spread and higher mean value – above the upper observational bound. Aerosol models are typically 'tuned' to have a plausible $\boldsymbol{\tau_{PD}}$ (although they appear to be biased low compared to these observations), while the PPE was designed to sample the full parametric uncertainty, and so this difference is not surprising. The higher range of values for $\boldsymbol{\tau_{PD}}$ shown in the PPE is due to the large base $\boldsymbol{\tau_{PD}}$ produced by the model (labelled 'default' in Fig.1) and the large range of uncertainty in sea-salt emissions elicited during the construction of the experiment.

A clear relationship between global annual mean $\boldsymbol{\tau_{ant}}$ and $\boldsymbol{\tau_{PD}}$ is evident in each of the ensembles and can be understood in simple physical terms. Firstly, it can be shown that the covariance between $\boldsymbol{X}$ and $\boldsymbol{X + Y}$, where $\boldsymbol{X}$ and $\boldsymbol{Y}$ are two normally distributed random variables, must be positive. The fact that both $\boldsymbol{\tau_{ant}}$ and $\boldsymbol{\tau_{PD}}$ are not independent and co-vary through shared removal mechanisms only increases this covariance. This is demonstrated by drawing samples from the simple analytic model for $\boldsymbol{\tau_{ant}}$ described by Charlson et al., 1992:

$$\boldsymbol{\tau_{ant} = \alpha_{SO_4} f(RH) Q_{SO_2} Y_{SO_4} L_{SO_4}/A,}$$

where the molar scattering cross section ($\boldsymbol{\alpha_{SO_4}}$), enhancement in scattering due to humidification ($\boldsymbol{f}$), anthropogenic sulfur dioxide source strength ($\boldsymbol{Q_{SO_2}}$), sulfate yield ($\boldsymbol{Y_{SO_4}}$), sulfate lifetime ($\boldsymbol{L_{SO_4}}$), and global area ($\boldsymbol{A}$) all have the same values and uncertainty estimates. We then extend this to estimate $\boldsymbol{\tau_{PD}}$ as:

$$\boldsymbol{\tau_{PD} = \alpha_{SO_4} f(RH)(Q_{SO_2} Y_{SO_4} + Q^n_{SO_4}) L_{SO_4}/A + \tau_{SS} + \tau_D + \tau_{OC},}$$

by including a natural sulfate source term ($\boldsymbol{Q^n_{SO_4}}$, with the same lifetime) and including natural sea-salt ($\boldsymbol{\tau_{SS}}$), dust ($\boldsymbol{\tau_D}$) and organic carbon ($\boldsymbol{\tau_{OC}}$) components from the distributions described in Bellouin et al., 2013. As shown in gray-scale contours of Figure 1, this distribution shows a very similar relationship to both ensembles and is in remarkably good agreement with the observations. While this simple model does not include many of the processes and uncertainties as the more complex PPE, it demonstrates the basis for the relationship between $\boldsymbol{\tau_{ant}}$ and $\boldsymbol{\tau_{PD}}$.

[2] A hex-density plot represents a 2D histogram using hexagonal bins – avoiding visual artefacts sometimes associated with square bins

Indeed, the parameters which were found to affect the shape of the PPE joint distribution the most were the scaling of sea-salt and anthropogenic sulfate emissions, and the parameter scaling removal through dry deposition (not shown) - the three key uncertainties in the simple model (where all removal terms are represented by an SO4 lifetime). While the anthropogenic emissions primarily affect $\boldsymbol{\tau_{ant}}$ and the sea salt emissions only affect $\boldsymbol{\tau_{PD}}$, the dry deposition affects both, providing the basis of the relationship in the PPE (see Figure S2). This allows an observational constraint on $\boldsymbol{\tau_{PD}}$ (0.14 to 0.17) to be translated into a constraint on $\boldsymbol{\tau_{ant}}$ (a 1σ range of approximately 0.03 to 0.05). Visually inspecting the overlap between the multi-model relationships and the observational range of $\boldsymbol{\tau_{PD}}$ provides a very similar range of $\boldsymbol{\tau_{ant}}$ of approximately 0.03-0.04.

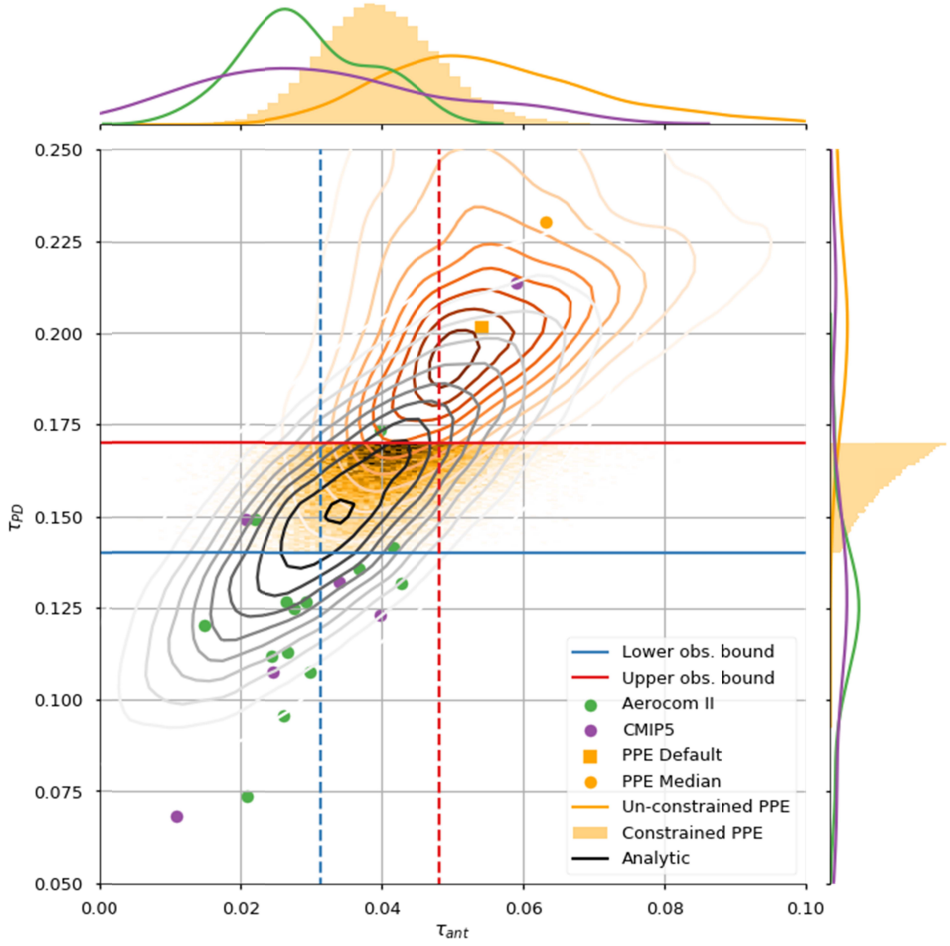

Figure 1: Distributions of the present-day aerosol optical depth, τ_{PD} against the industrial-era change in aerosol optical depth at 0.55μm, τ_{ant}, between pre-industrial and present-day, from AeroCom Phase II and CMIP5 sstClimAerosol models. The full joint-probability distribution sampled from the emulated HadGEM-UKCA 26 aerosol parameter PPE is shown as contour lines, and the constrained distribution as a hex-density. The default and median model runs of the PPE are also shown for completeness. The grey-scale contour lines show the joint distribution

sampled from an analytic approximation described in the main text. The horizontal lines show the 1σ observational uncertainty range in globally-averaged τ_{PD}, while the vertical lines show the resulting 1σ range in τ_{ant} of the constrained PPE.

Clear-sky RF_{ari} against τ_{ant} for the same model ensembles is shown in Fig. 2. The full joint-probability distribution from the emulated PPE is shown with contour lines, while the values constrained by the τ_{PD} observations are shown as a hex-density. The effect of the constraint of the τ_{PD} on the spread in uncertainty in both τ_{ant} and RF_{ari} is immediately obvious. The full distribution of RF_{ari} in the model variants sampled from the emulated PPE peaks at -0.8 W m^{-2} and is non-negligible even at -1.2 W m^{-2}. After applying the constraint, the remaining variants provide a 1σ range in clear-sky RF_{ari} of -0.54 – -0.8 W m^{-2}. This is very similar to the original AeroCom range (-0.47 – -0.84 W m^{-2}), and a similar range to that which would be provided by assuming a linear relationship in both the AeroCom and CMIP5 ensembles (-0.7 – -0.85 W m^{-2}) using the values of $\boldsymbol{\tau_{ant}}$ derived above. The RF_{ari} is directly proportional to τ_{ant} (Charlson et al., 1992) and this is demonstrated by the excellent agreement in clear-sky forcing efficiencies $\frac{RF_{ARI}}{\tau_{ant}}$ among all three ensembles. All of which are in-line with the values for the AeroCom models reported by Myhre et al., 2013 of -23.7 $\pm$ 3.1 $Wm^{-2}\tau^{-1}$ (neglecting an anomalous outlier).

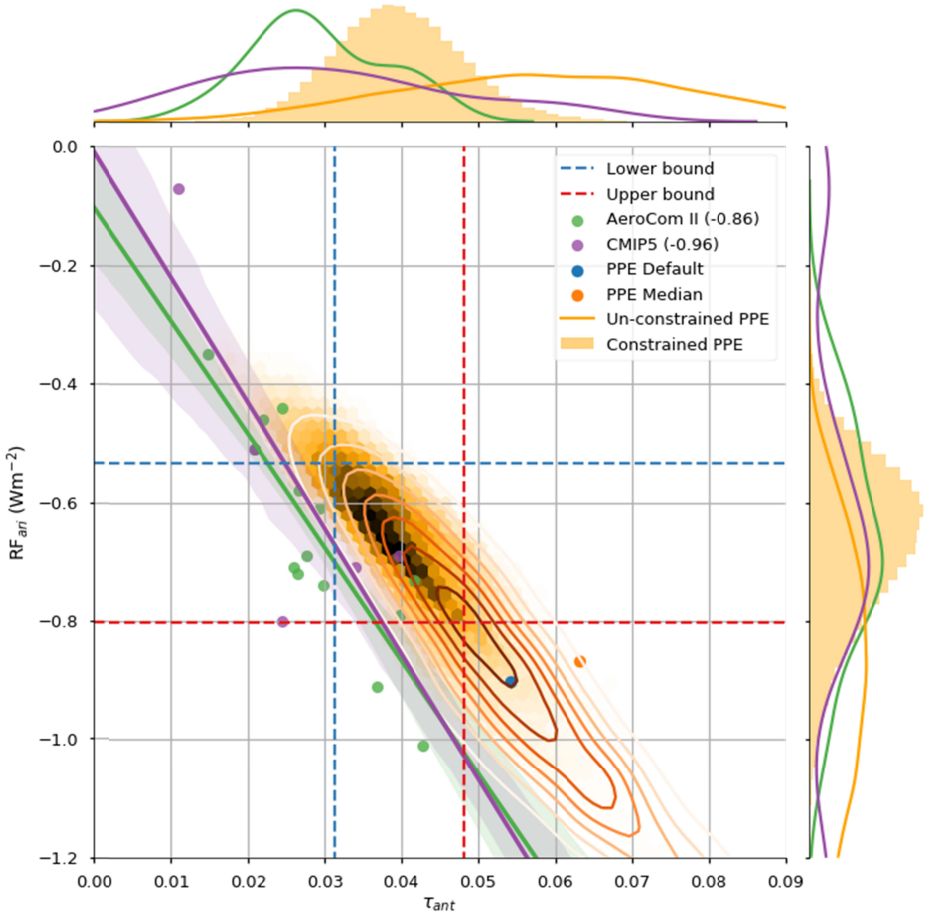

Figure 2: Clear-sky radiative forcing of aerosol-radiation interactions, RFari in Wm-2, as a function of the industrial-era change in aerosol optical depth at 0.55 μm, τ_{ant} in AeroCom models (green) and CMIP5 models (purple). The slopes of the lines of best fit for each dataset are -19.1 and -21Wm^{-2} τ^{-1}, respectively. The joint-distribution of the full emulated PPE is shown with contours, while the samples consistent with τ_{PD} is shown as a hex-density. The default and median model runs are also shown for completeness. The 1σ uncertainty in the fits are shaded and the correlation coefficients are indicated in the parentheses in the legend. The 1σ ranges in τ_{ant} and RFari from the constrained PPE are indicated by the vertical and horizontal lines respectively.

Within this framework we can ask what effect a reduction in the observational uncertainty in τ_{PD} would have on reducing the uncertainty in RF_{ari} from the PPE even further. Figure 3 shows the uncertainty (1σ spread in the constrained emulated samples) in RF_{ari} as a function of lower and upper observational bounds on τ_{PD}. Naively, the uncertainty might be expected to decrease closer to the diagonal where the observational uncertainty is smallest. However, the largest control on the uncertainty in the RFari as constrained through τ_{PD} is actually the magnitude of the upper bound. This reflects the shape of the joint probability distribution in Fig.1 where the lower bound is already on the edge of the plausible values from the PPE, whereas the upper bound intersects the peak of the probability distribution. Intuitively this can be understood as the τ_{PD} containing less information about the anthropogenic aerosol as the magnitude increases, as there is more flexibility in how the total is partitioned between anthropogenic and seasalt.

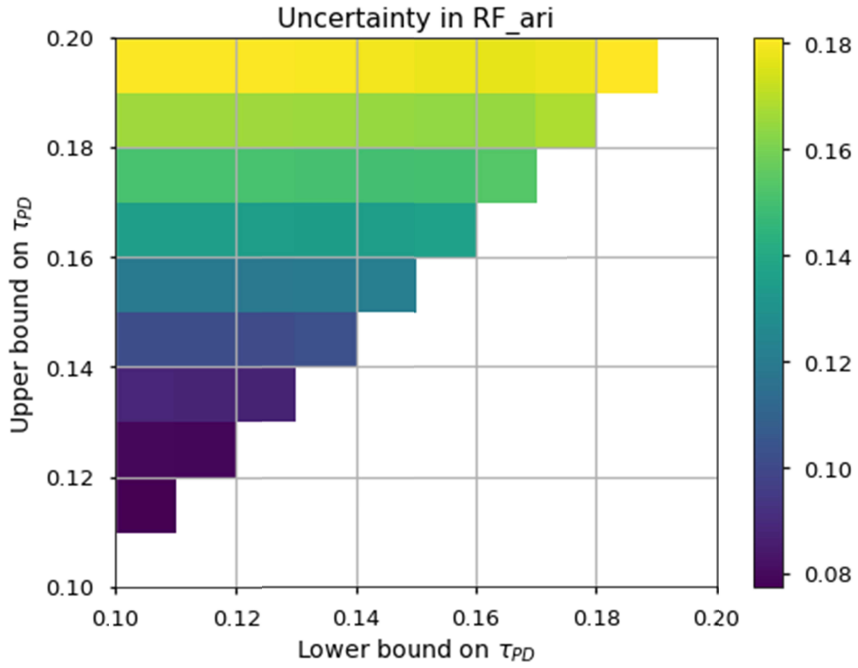

Figure 3: The standard deviation in RFari sampled from the emulated HadGEM3-UKCA aerosol PPE for different lower and upper bounds on the corresponding emulated τ_{PD}.

3 Discussion

The anthropogenic contribution to the present-day aerosol loading has been a key source of uncertainty in both bottom-up and top-down estimates of the aerosol forcing. We have demonstrated a robust relationship between present-day total and anthropogenic aerosol loading across two multi-model ensembles and a perturbed parameter ensemble. Combined with observational bounds on the total present-day aerosol loading we estimate $\boldsymbol{\tau_{ant}}$ to be in the 1σ range 0.031 - 0.048 (or a 95% credible range of 0.026 – 0.054). For comparison, by determining the anthropogenic contribution to fine mode aerosol in the Monitoring Atmospheric Composition and Climate (MACC) Reanalysis (Benedetti et al. 2009), Bellouin et al. 2013 determine $\boldsymbol{\tau_{ant}}$ as 0.06. This is slightly higher than our estimate, potentially due to relying on the MODIS retrieved $\boldsymbol{\tau}$ which are two of the largest values used in our observational dataset. The Max Planck Institute Aerosol Climatology (MAC) (Kinne et al., 2006) combines AERONET climatologies with aerosol properties from AeroCom models (Kinne et al., 2006) and report $\boldsymbol{\tau_{ant}}$ of 0.03, which is in good agreement with our estimate.

The plausible range in $\boldsymbol{\tau_{ant}}$ translates into a constrained clear-sky RF_{ari} of -0.67 ± 0.13 Wm^{-2} (or a 95% credible range of -0.91 – -0.47 Wm^{-2}). Although this range is not significantly smaller than the original ranges demonstrated in the AeroCom (Myhre et al., 2013) and CMIP5 (Zelinka et al., 2014) ensembles, these were not sampling the full model uncertainty, as demonstrated by the large uncertainty in the unconstrained PPE forcing for HadGEM-UKCA (-0.91 ± 0.23 Wm^{-2}, or 95% range of 1.32 – -0.56 Wm^{-2}). While performing similar PPE experiments for each of the models in the AeroCom and CMIP5 ensembles would reveal the full, presumably larger, uncertainty in RF_{ari}, the robust relationship between the base models suggests this constraint may hold. We have also explored the sensitivity of this constraint to the observational uncertainty in $\boldsymbol{\tau_{PD}}$. The constraint is much more sensitive to the upper bound, rather than the spread and so a robust estimate of this upper bound should be the focus for future investigation. It is also possible that other retrieved properties, such as fine mode AOD or multiple-wavelength AOD would provide a tighter constraint.

While all the model ensembles are in good agreement on the clear-sky forcing efficiencies, there is still uncertainty around the magnitude of aerosol absorption, and in particular the absorptivity of black carbon (BC). Indeed, this PPE did not explore the large uncertainty in the imaginary part of the refractive index of BC. By combining the AOD constraint with observations of absorbing AOD it may be possible to better constrain the magnitude of aerosol absorption. Future work will use absorbing AOD measurements to constrain the RFari, including the (large) uncertainty in these particles. The radiative forcing due to aerosol-cloud interactions (RF_{aci}) depends logarithmically on $\boldsymbol{\tau_{ant}}$ and so is even more sensitive to its uncertainty than RF_{ari} (Carslaw et al., 2013). Despite AOD being an unreliable proxy for cloud condensation nuclei (Stier, 2016), a constraint on anthropogenic fraction should be expected to constrain the anthropogenic contribution to CCN, and hence help constrain RF_{aci}. Future work will explore this possibility.

Acknowledgments

DWP and PS acknowledge support from the NERC CLouds and Aerosol Radiative Impacts and Forcing: Year 2016 (CLARIFY-2016, NE/L013746/1) project. PS additionally acknowledges support from the European Research Council (ERC) project constRaining the EffeCts of Aerosols on Precipitation (RECAP) under the European Union's Horizon 2020 research and innovation program with grant agreement No 724602 and the Alexander von Humboldt Foundation. This research was funded by the Natural Environment Research Council (NERC) under grants NE/J024252/1 (GASSP), NE/I020059/1 (ACID-PRUF) and NE/P013406/1 (A-CURE), the National Centre for Atmospheric Science (DWP, LD, MY, KC, PS); and the UK–China Research and Innovation Partnership Fund through the Met Office Climate Science for Service Partnership (CSSP) China as part of the Newton Fund (JJ, KC, LR). We made use of the N8 HPC facility funded from the N8 consortium and an Engineering and Physical Sciences Research Council Grant to use ARCHER (EP/K000225/1) and the JASMIN facility (http://www.jasmin.ac.uk/, last access: 4 September 2018) via the Centre for Environmental Data Analysis, funded by NERC and the UK Space Agency and delivered by the Science and Technology Facilities Council. We acknowledge the following additional funding: The Royal Society Wolfson Merit Award (KC), a doctoral training grant from the Natural Environment Research Council and a CASE studentship with the Met Office Hadley Centre (LR). We also gratefully acknowledge the support of Amazon Web Services through an AWS Machine Learning Research Award.

We thank Stephan Kinne and Dave Winker for useful discussions.

Data availability

The CMIP5 values are available as a supplementary table to Zelinka et al., 2014. The AeroCom II data is read directly from the tables in Myhre et al. 2013. Raw simulation output data from the HadGEM-UKCA PPE ensembles are available as Met Office postprocessing data format (.pp; Met Office, 2013) from the JASMIN data infrastructure (http://www.jasmin.ac.uk).Some of the climate-relevant fields are derived and stored in netCDF files (.nc) containing data for all ensemble members and made available as a community research tool. The total data sizes are around 85 TB.

References

Bellouin, N., Quaas, J., Morcrette, J.-J., & Boucher, O. (2013). Estimates of aerosol radiative forcing from the MACC re-analysis. *Atmospheric Chemistry and Physics*, *13*(4), 2045–2062. https://doi.org/10.5194/acp-13-2045-2013

Benedetti, A., Morcrette, J. -J., Boucher, O., Dethof, A., Engelen, R., Fisher, M., et al. (2009). Aerosol analysis and forecast in the European Centre for Medium-Range Weather Forecasts Integrated Forecast System: 2. Data assimilation. *Journal of Geophysical Research: Atmospheres (1984–2012)*, *114*(D13). https://doi.org/10.1029/2008jd011115

Carslaw, K., Lee, L., Reddington, C., Pringle, K., Rap, A., Forster, P., et al. (2013). Large contribution of natural aerosols to uncertainty in indirect forcing. *Nature*, *503*(7474), 67. https://doi.org/10.1038/nature12674

Carslaw, K. S., Gordon, H., Hamilton, D. S., Johnson, J. S., Regayre, L. A., Yoshioka, M., & Pringle, K. J. (2017). Aerosols in the Pre-industrial Atmosphere. *Current Climate Change Reports*, *3*(1), 1–15. https://doi.org/10.1007/s40641-017-0061-2

Charlson, R., Schwartz, S., Hales, J., Cess, R., Coakley, J., Hansen, J., Hofmann, D. (1992). Climate Forcing by Anthropogenic Aerosols. *Science* 255(5043), 423-430. https://dx.doi.org/10.1126/science.255.5043.423

Dunne, E. M., Gordon, H., Kürten, A., Almeida, J., Duplissy, J., Williamson, C., et al. (2016). Global atmospheric particle formation from CERN CLOUD measurements. *Science*, *354*(6316), 1119–1124. https://doi.org/10.1126/science.aaf2649

Hall, A., & Qu, X. (2006). Using the current seasonal cycle to constrain snow albedo feedback in future climate change. *Geophysical Research Letters*, *33*(3).

N. C. Hsu, A. M. Sayer, M.-J. Jeong, and C. Bettenhausen (2013), SeaWiFS Deep Blue Aerosol Optical Depth and Angstrom Exponent Level 2 Data V004, Greenbelt, MD, USA, Goddard Earth Sciences Data and Information Services Center (GES DISC), 10.5067/MEASURES/SWDB/DATA201

Kinne, S., Schulz, M., Textor, C., Guibert, S., Balkanski, Y., Bauer, S., et al. (2006). An AeroCom initial assessment – optical properties in aerosol component modules of global models. *Atmospheric Chemistry and Physics*, *6*(7), 1815–1834. https://doi.org/10.5194/acp-6-1815-2006

Klein, S. A., & Hall, A. (2015). Emergent Constraints for Cloud Feedbacks. *Current Climate Change Reports*, *1*(4), 276–287. https://doi.org/10.1007/s40641-015-0027-1

Kolmonen, P.; Sogacheva, L.; Timo, H.; Virtanen, T.H.; de Leeuw, G.; Kulmala, M. The ADV/ASV AATSR aerosol retrieval algorithm: Current status and presentation of a full-mission AOD dataset. Int. J. Digit. Earth 2016, 9, 545–561.

Lee, L., Reddington, C., Carslaw, K. (2016). On the relationship between aerosol model uncertainty and radiative forcing uncertainty. https://dx.doi.org/10.1073/pnas.1507050113

Lee, L., Pringle, K., Reddington, C., Mann, G., Stier, P., Spracklen, D., et al. (2013). The magnitude and causes of uncertainty in global model simulations of cloud condensation nuclei. *Atmospheric Chemistry and Physics*, *13*(17), 8879–8914. https://doi.org/10.5194/acp-13-8879-2013

Levy, R.C.; Mattoo, S.; Munchak, L.A.; Remer, L.A.; Sayer, A.M.; Patadia, F.; Hsu, N.C. The Collection 6 MODIS aerosol products over land and ocean. Atmos. Meas. Tech. 2013, 6, 2989–303

Matthews, A., , e., Wilk, M., Nickson, T., Fujii, K., Boukouvalas, A., Leon-Villagra, P., Ghahramani, Z., Hensman, J. (2017). GPflow: A Gaussian process library using TensorFlow Journal of Machine Learning Research 18(40), 1-6.

Myhre G, D, W, J, J, et al. (2013). Climate Change 2013: The Physical Science Basis. Contribution of Working Group I to the Fifth Assessment Report of the Intergovernmental Panel on Climate Change.

Myhre, G., Samset, B., Schulz, M., Balkanski, Y., Bauer, S., Berntsen, T., et al. (2013). Radiative forcing of the direct aerosol effect from AeroCom Phase II simulations. *Atmospheric Chemistry and Physics*, *13*(4), 1853–1877. https://doi.org/10.5194/acp-13-1853-2013

Nocedal, J, and S J Wright. 2006. Numerical Optimization. Springer New York.

Stier, P. (2016). Limitations of passive remote sensing to constrain global cloud condensation nuclei. *Atmospheric Chemistry and Physics*, *16*(10), 6595–6607. https://doi.org/10.5194/acp-16-6595-2016

Taylor, K. E., Stouffer, R. J., & Meehl, G. A. (2012). An Overview of CMIP5 and the Experiment Design. *Bulletin of the American Meteorological Society*, *93*(4), 485–498. https://doi.org/10.1175/bams-d-11-00094.1

Thomas, G.E.; Carboni, E.; Sayer, A.M.; Poulsen, C.A.; Siddans, R.; Grainger, R.G. Oxford-RAL Aerosol and Cloud (ORAC): Aerosol retrievals from satellite radiometers. In Aerosol Remote Sensing over Land; Kokhanovsky, A., de Leeuw, G., Eds.; Springer: Berlin/Heidelberg, Germany, 2009; pp. 193–225.

Yoshioka, M., Regayre, L. A., Pringle, K. J., Johnson, J. S., Mann, G. W., Partridge, D. G., et al. (2019): Ensembles of Global Climate Model Variants Designed for the Quantification and Constraint of Uncertainty in Aerosols and their Radiative Forcing, J. Adv. Model. Earth Syst., 11, 11, 3728– 3754. DOI: 10.1029/2019MS001628

Zelinka, M. D., Andrews, T., Forster, P. M., & Taylor, K. E. (2014). Quantifying components of aerosol-cloud-radiation interactions in climate models. *Journal of Geophysical Research: Atmospheres*, *119*(12), 7599–7615. https://doi.org/10.1002/2014jd021710